Supplemental Material for "Observation of an edge-to-edge topological transport in photonic lattice"

Weijie Liu[1,*], Chaohua Wu[2,3*], Yuechen Jia[1], Suotang Jia[2,3], Gang Chen[2,3,4†], and Feng Chen[1,†]

[1]School of Physics, State Key Laboratory of Crystal Materials, Shandong University, Jinan, 250100, China

[2]State Key Laboratory of Quantum Optics and Quantum Optics Devices, Institute of Laser spectroscopy, Shanxi University, Taiyuan 030006, China

[3]Collaborative Innovation Center of Extreme Optics, Shanxi University, Taiyuan, Shanxi 030006, China

[4]Collaborative Innovation Center of Light Manipulations and Applications, Shandong Normal University, Jinan 250358, China

*These authors contributed equally to this work.

†Corresponding author: chengang971@163.com; drfchen@sdu.edu.cn

This Supplemental Material includes:

SM-I. Topologically-protected edge state for the odd-sized SSH model

In the momentum space, the Hamiltonian (1) of the main text is rewritten as

$$H(k)=\begin{pmatrix}0 & J_1+J_2e^{-ik}\\ J_1+J_2e^{ik} & 0\end{pmatrix}. \tag{S1}$$

By solving an eigenequation

$$H(k)|\psi(k)\rangle=E(k)|\psi(k)\rangle, \tag{S2}$$

we obtain the eigenvalues

$$E_{\pm}(k)=\pm\sqrt{J_1^2+J_2^2+2J_1J_2\cos(k)}, \tag{S3}$$

with eigenstates $|\psi_{\pm}(k)\rangle=\left[E_{\pm}(k)/(J_1+J_2e^{-ik}),1\right]^T/\sqrt{2}$, where T denotes the

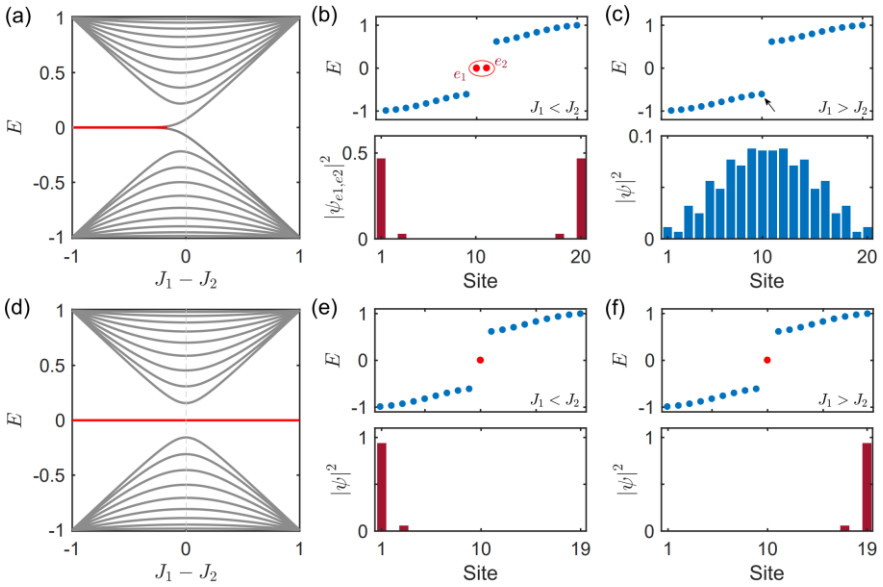

Figure S1. (a) Energy spectrum of the SSH lattice with 20 sites versus $J_1 - J_2$. (b) Energy spectrum (upper panel) and density distribution of the zero-energy edge state (lower panel) for $J_1 = 0.2$ and $J_2 = 0.8$. (c) Energy spectrum (upper panel) and density distribution of one bulk state (lower panel) for $J_1 = 0.8$ and $J_2 = 0.2$. (d)-(f) show energy spectrum and edge state for 19 sites with the same J_1 and J_2 as those in (a)-(c). In all subfigures, we assume $J_1 + J_2 = 1$ ($J_{1,2} > 0$) and set it as the energy unit.

transposition of the matrix. The Hamiltonian (S1) exhibits two topologically distinct phases associated with two configurations, $J_1 > J_2$ and $J_1 < J_2$, separated by a topological phase transition point at $J_1 = J_2$. The different topologies of these two phases are characterized by the winding number $\nu_\pm = \frac{i}{\pi}\int_{-\pi}^{\pi}\langle\psi_\pm(k)|\partial_k\psi_\pm(k)\rangle$. For $J_1 < J_2$ ($J_1 > J_2$), $\nu_\pm = 1$ ($\nu_\pm = 0$). The topological phase transition is protected by the chiral symmetry of the system, since $\Gamma H \Gamma^{-1} = -H$, where the chiral operator $\Gamma = \sigma_z \otimes \mathbb{I}$ with σ_z and $\mathbb{I}$ being the Pauli and identity matrices.

According to the bulk-edge correspondence, the SSH lattice exhibits zero-energy edge states in the bulk gap. For the even-sized lattice with $2N$ sites, the nontrivial topological phase hosts two edge states localized on the boundary of the lattice, as shown in Figs. S1(a)-S1(c). On the contrary, for the odd-sized lattice with $2N - 1$ sites, there is always one edge state, whose localized position depends crucially on J_1 and J_2, as shown in Figs. S1(d)-S1(f).

Analytically, the zero-energy eigenstate for the odd-sized lattice can be obtained by solving

$$H\sum_n(a_n|n,A\rangle + b_n|n,B\rangle) = 0, \tag{S4}$$

where a_n and b_n are the amplitudes in the n-th unit cell. Substituting the Hamiltonian (1) of the main text into Eq. (S4), we have

$$J_1 a_n + J_2 a_{n+1} = 0, \quad (n = 1, \dots, N-1), \tag{S5a}$$

$$J_2 b_n + J_1 b_{n+1} = 0, \quad (n = 1, \dots, N-2). \tag{S5b}$$

In terms of the boundary conditions

$$J_1 b_1 = 0, \; J_2 b_N = 0, \tag{S6}$$

the zero-energy edge state is derived as

$$\begin{cases} |\psi_l\rangle = \mathcal{N}_l \sum_n \left(-\frac{J_1}{J_2}\right)^{n-1} |n, A\rangle, & (J_1 < J_2) \\ |\psi_r\rangle = \mathcal{N}_r \sum_n \left(-\frac{J_2}{J_1}\right)^{N-n} |n, A\rangle, & (J_1 > J_2) \end{cases}, \tag{S7}$$

where the normalized coefficients $\mathcal{N}_l = \sqrt{[(J_1/J_2)^2 - 1]/[(J_1/J_2)^{2N} - 1]}$ and $\mathcal{N}_r = \sqrt{[(J_2/J_1)^2 - 1]/[(J_2/J_1)^{2N} - 1]}$, and $n = 1, \dots, N$. Equation (S7) shows clearly that when $J_1 < J_2$ $(J_1 > J_2)$, the edge state is localized in the left (right) side of the lattice and only occupies the A sites. At $J_1 = J_2$, this zero-energy state is fully delocalized along the lattice.

SM-II. Adiabatic pumping of edge state in the odd-sized SSH model

It can be found from Eq. (S7) that for the odd-sized SSH model, only one edge state always exits and its localized position depends on J_1 and J_2, as shown in Figs. S1(d)-S1(f). As a result, we can realize the topologically-protected transfer of light by adiabatically pumping the edge state from one side to the other (i.e., edge-to-edge topological transport). This can be achieved by properly modulating J_1 and J_2.

As shown in Fig. S2(a), the system is initially prepared with $J_1(z = 0) = 0$ and $J_2(z = 0) = J_m$, where J_m is the maximum value of both the modulated J_1 and J_2. Moreover, the injected light is localized at the leftmost waveguide, which overlaps with the zero-energy edge state $|\psi(z = 0)\rangle = |1, A\rangle$ in Fig. S2(b). Then, by slowly varying the coupling strengths from $J_1/J_2 < 1$ to $J_1/J_2 > 1$, the light propagates adiabatically from $|\psi_l\rangle$ to $|\psi_r\rangle$ along the zero-energy eigenstates, as shown in Figs. S2(c)-S2(e). Finally, the coupling strengths have $J_1(z = L) = J_m$ and $J_2(z = L) = 0$, at which the light arrives at the rightmost waveguide with the zero-energy edge state $|\psi(z = L)\rangle = |N, A\rangle$ in Fig. S2(f). We emphasize that this adiabatic transport of light along the zero-energy eigenstates only occupying the A sites is topologically protected by a band gap (Δ) between the zero-energy and its adjacent eigenstates [see Fig. S2(a)] due to the

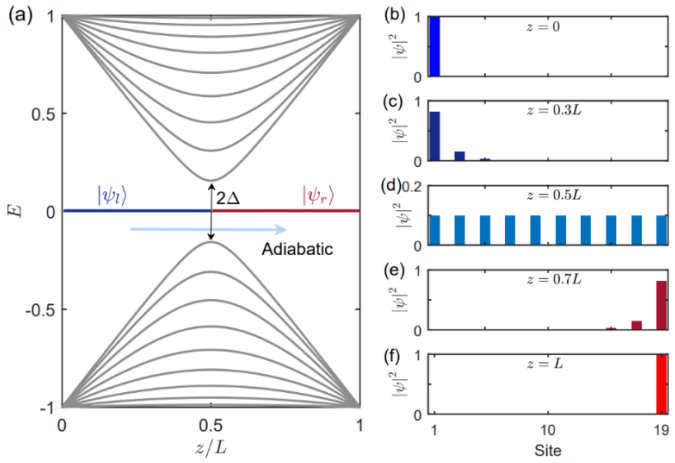

Figure S2. (a) Schematic of the adiabatic pumping of the zero-energy edge state for the SSH model with 19 sites. The state evolves adiabatically from $|\psi_l\rangle$ to $|\psi_r\rangle$ along the zero-energy eigenstates. Δ is the gap between the zero-energy and its adjacent eigenstates. (b)-(f) Density distributions of the zero-energy eigenstates for $z=0$ (b), $z=0.3L$ (c), $z=0.5L$ (d), $z=0.7L$ (e), and $z=L$ (f). Here we choose $J_1(z)=z/L$ and $J_2(z)=1-z/L$. Here, we set $\max\{J_{1,2}(z)\}=1$ as the energy unit.

system's finite size and thus offers immunity against scattering from disorders and imperfections.

Treated z as a virtual time, the adiabatic evolution of light is governed by the following Schrödinger-type equation:

$$-i\partial_z|\psi(z)\rangle = H(z)|\psi(z)\rangle, \tag{S8}$$

where $|\psi(z)\rangle$ denotes the instantaneous eigenstate for the time-dependent Hamiltonian $H(z)$. The wavefunction can be expanded as

$$|\psi(z)\rangle = \sum_l c_l e^{-iE_l z}|\psi_l(z)\rangle, \quad (l=-N,\dots,0,\dots N), \tag{S9}$$

where $|\psi_l(z)\rangle$ and E_l are the instantaneous eigenvectors and eigenvalues obeying an eigenequation $H(z)|\psi_l(z)\rangle = E_l|\psi_l(z)\rangle$. Substituting Eq. (S9) into Eq. (S8), we obtain

$$\frac{\partial c_l}{\partial z} = \sum_{l'\neq l} c_{l'} e^{-i(E_{l'}-E_l)z} \frac{\langle\psi_l|\partial H(z)/\partial z|\psi_{l'}\rangle}{E_{l'}-E_l}. \tag{S10}$$

From Eq. (S10), it follows that in order to approach the adiabatic limit, we have

$$\sum_{l'\neq l} \frac{1}{E_{l'}-E_l}\left\langle\psi_l\left|\frac{\partial H(z)}{\partial z}\right|\psi_{l'}\right\rangle \ll 1. \tag{S11}$$

That is to say, the adiabatic condition requires that the energy gap $E_{l'}-E_l$ is large enough or the Hamiltonian varies slowly. For the odd-sized SSH model with $2N-1$ sites, the energy gap between the zero-energy ($l=0$) and its adjacent eigenstates can

be derived analytically as [S1]

$$\Delta = \left| J_1 + J_2 e^{i\pi(N-1)/N} \right|, \tag{S12}$$

which has a minimum value $\Delta_{\min}$ at $J_1 = J_2$.

According to Eq. (S11), the adiabatic condition requires that the temporal variation of the system Hamiltonian should be much slower than energy gap between the edge and bulk states. For the most schemes of topological transport, such as Thouless pumping, the energy gap between the edge states and bulk states becomes small during the evolution. This means that the temporal variation of the system Hamiltonian is extremely slow. To enhance the speed and efficiency of the edge-to-edge topological transport proposed here, we have following two considerations. One is to increase $\Delta_{\min}$, which can be achieved by forcing J_1 and J_2 to be equal at a large value. We can safely assume that the evolution is closed to the adiabatic if $\Delta_{\min}$ is sufficiently large compared to the temporal variation of $H(z)$. The other is that when Δ is bigger, we strongly drive the system with steeper slop of J_1 and J_2, and when close to $\Delta_{\min}$, they become more gentle with smaller slope. In Sec. SM-III, we choose the proper J_1 and J_2 to balance the interplay between the two aforementioned considerations.

SM-III. Choice of the modulating coupling strengths

In Fig. S3, we plot three kinds of the modulating coupling strengths, $J_1 = 0.5[1-\cos(\pi z/L)]$ and $J_2 = 0.5[1+\cos(\pi z/L)]$ (a), $J_1 = \sin[\pi z/(2L)]$ and $J_2 = \cos[\pi z/(2L)]$ (b), and $J_1 = \left(1-e^{-\alpha z/L}\right)/(1-e^{-\alpha})$ and $J_2 = \left[1-e^{-\alpha(L-z)/L}\right]/(1-e^{-\alpha})$ (c) with the fine-tuned parameter $\alpha = 4$. This figure shows that for the exponential modulations, the intersection (blue circle) of J_1 and J_2

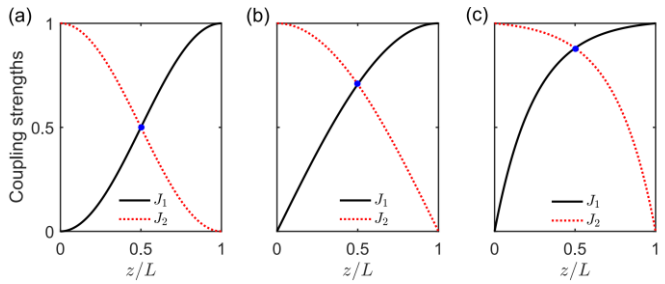

Figure S3. Plot of three kinds of the modulating coupling strengths, $J_1 = 0.5[1-\cos(\pi z/L)]$ and $J_2 = 0.5[1+\cos(\pi z/L)]$ (a), $J_1 = \sin[\pi z/(2L)]$ and $J_2 = \cos[\pi z/(2L)]$ (b), and $J_1 = \left(1-e^{-\alpha z/L}\right)/(1-e^{-\alpha})$ and $J_2 = \left[1-e^{-\alpha(L-z)/L}\right]/(1-e^{-\alpha})$ (c) with $\alpha = 4$. Blue circles denote the intersections of J_1 and J_2. Here, we set $\max\{J_{1,2}(z)\} = 1$ as the energy unit.

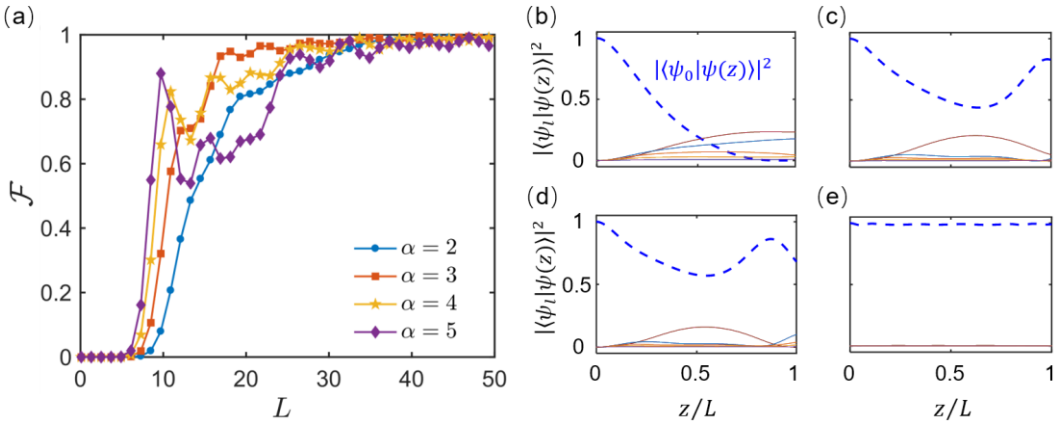

Figure S4. (a) Transport efficiencies $\mathcal{F}$ as functions of L for $J_1 = \left(1 - e^{-\alpha z/L}\right)/(1 - e^{-\alpha})$ and $J_2 = \left[1 - e^{-\alpha(L-z)/L}\right]/(1 - e^{-\alpha})$, when $\alpha = 2$, 3, 4, and 5. (b)-(e) Populations of eigenstates, $|\langle\psi_l(z)|\psi(z)\rangle|^2$, as functions of z for $L = 3$ (b), 11 (c), 13 (d), and 60 (e), when $\alpha = 4$. In all subfigures, the site is chosen as 11 and $\max\{J_{1,2}(z)\} = 1$ is set as the energy unit.

has a large value, which amounts to a large $\Delta_{\min}$, and moreover, they have steeper slope for a larger Δ. As a result, the exponential modulations are the qualified candidates to achieve fast topologically-protected transport of light.

In Fig. S4(a), we further plot the transport efficiencies [see Eq. (3) of the main text] for the exponential modulations as functions of L, when $\alpha = 2$, 3, 4, and 5. This figure shows that when $\alpha \leq 3$, the transport efficiency increases monotonously with the increasing of L. When $\alpha > 3$, the transport efficiency is featured by oscillation and is moreover reduced in the intermediate L. To illustrate this oscillation behavior, we take $\alpha = 4$ as an example. In Figs. S4(b)-S4(e), we plot the populations of eigenstates, $|\langle\psi_l(z)|\psi(z)\rangle|^2$, as functions of z for different L. For a small L, the population of the zero-energy eigenstate ($|\psi_0\rangle$) transits quickly to other eigenstates and fails to return; see Fig. S4(b). For the intermediate L, the population oscillates between $|\psi_0\rangle$ and other eigenstates; see Figs. S4(c) and S4(d). Moreover, due to the interference between $|\psi_0\rangle$ and other excited states [S2], the transport efficiency reduces. For a large L, the state $|\psi(z)\rangle$ is "frozen" on $|\psi_0\rangle$ without exciting other eigenstates, as shown in Fig. S4(e), i.e., the adiabatic transport of light can be realized perfectly.

Based on above analysis, we experimentally choose $\alpha = 3$ of the exponential modulations, since it ensures that the system posseses a high transport speed without exhibiting stong oscillation effects.

SM-IV. Implementation of the modulated coupling strengths

To modulate J_1 and J_2, we vary intracell and intercell spacings (d_1 and d_2) between the adjacent waveguides, which can be implemented by continuously moving the sample through a high-precision system. Note that in our photonic waveguides with the 633 nm injected laser (see the main text for more details), there exists a general relation between the coupling strength and the spacing [S3]:

$$J = \eta e^{\gamma d}, \tag{S13}$$

where η and γ are the parameters to be determined as follows. We fabricate a series of two-waveguide systems with the same $L = 9.6$ mm but $d \in [12, 24]$ μm with an interval of 2 μm. In Fig. S5(a), we measure the outgoing intensity distributions of light at the output. Since the light intensity in the left waveguide satisfies an equation $I = I_0 \cos^2(Jz)$, where I_0 is the total light intensity [S4], the relation of J with respect to d is given in Fig. S5(b). Finally, in terms of the fitting curve, we have $\eta = 3451$ m^{-1} and $\gamma = -0.2238$ μm^{-1}.

Figure S6(a) shows the variations of d_1 and d_2 with respect to z. Based on this figure and Eq. (13), we realize the exponential-type coupling strengths as

$$J_1 = \mathcal{J}\left[0.1 + 0.8\,(1 - e^{-3z/L})/(1 - e^{-3})\right], \tag{S14a}$$

$$J_2 = \mathcal{J}\left\{0.1 + 0.8\left[(1 - e^{-3(L-z)/L})\right]/(1 - e^{-3})\right\}, \tag{S14b}$$

where $\mathcal{J} = 1000$ m^{-1}. Note that in order to avoid loss caused by the large bending of the waveguides, the minimum and maximum spacings are set to 6 and 16 μm, respectively, i.e., J_1 and J_2 have added a factor of 0.1, compared with the theoretical

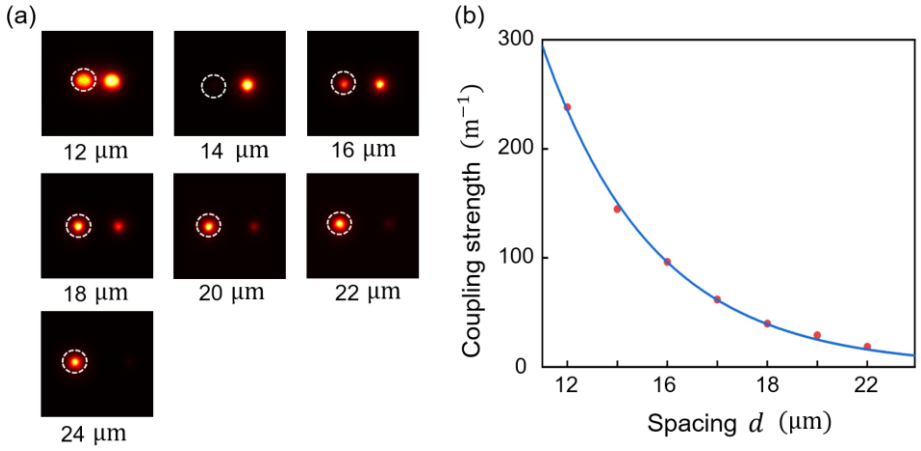

Figure S5. (a) Measured outgoing intensity distributions of light at the output for $d \in [12, 24]$ μm with an interval of 2 μm. (b) Measured coupling strengths (red dots). The blue solid line shows the fitting curve.

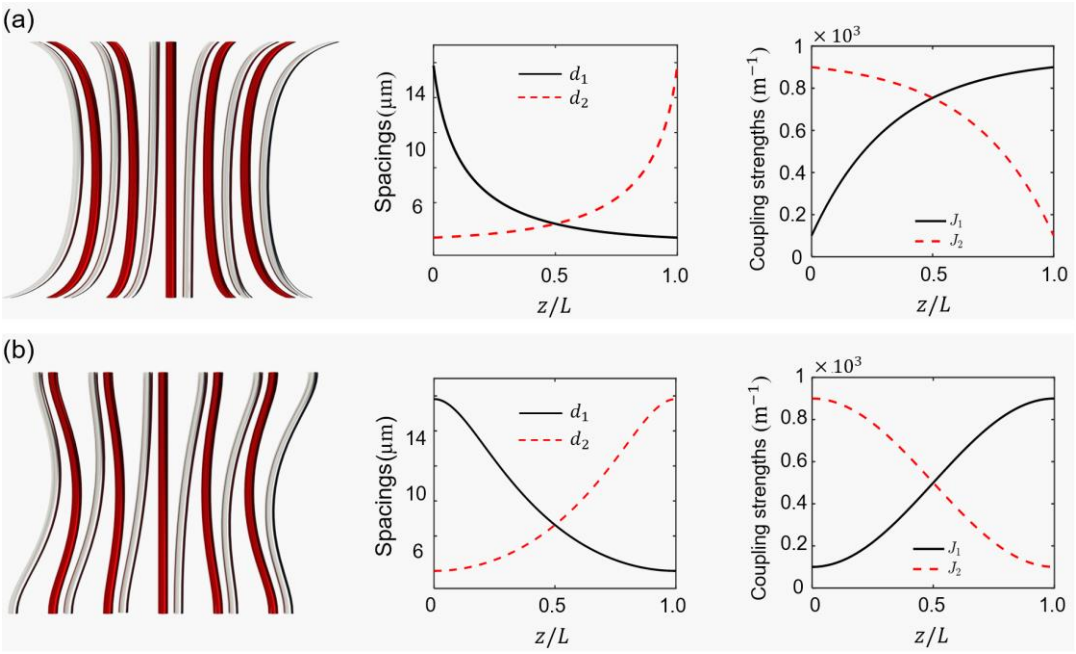

Figure S6. (a) Schematic of the waveguide array structure (left panel), the spacings d_1 and d_2 (middle), and the coupling strengths J_1 and J_2 (right panel) for the exponential modulations. The red dashed and black solid curves show respectively the intercell and intracell spacings and the corresponding coupling strengths. (b) The same as (a) but for the cosine modulations.

proposal in SM-III. Figure S6(b) shows the other variations of d_1 and d_2 with respect to z, from which the cosine-type coupling strengths are obtained by

$$J_1 = \mathcal{J}\{0.1 + 0.4[1 - \cos(\pi z/L)]\}, \tag{S15a}$$

$$J_2 = \mathcal{J}\{0.1 + 0.4[1 + \cos(\pi z/L)]\}. \tag{S15b}$$

SM-V. Energy spectra of the fabricated photonic waveguides

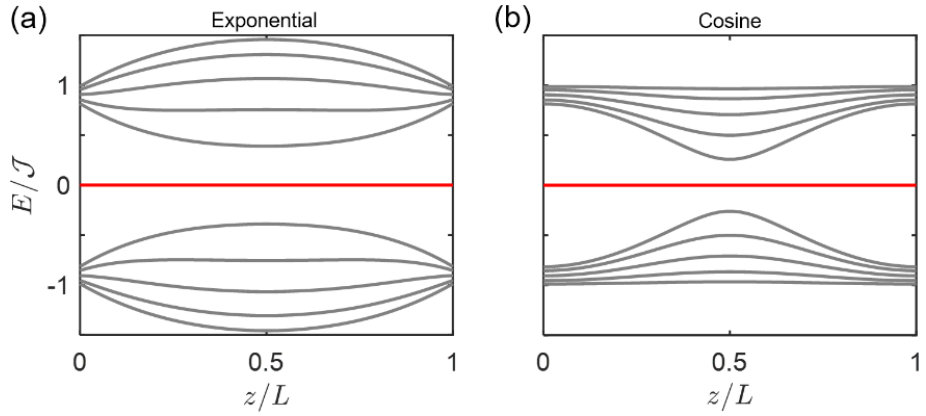

Figure S7. Energy spectra of the fabricated photonic waveguides with the exponential [Eq.(S14)] (a) and cosine [Eq.(S15)] (b) modulations of the coupling strengths. The site is chosen as 11.

SM-VI. Disorder analysis

In the presence of the coupling strength disorders (i.e., off-diagonal disorder), the perturbed Hamiltonian (5) in the main text still obeys the chiral symmetry, since $\Gamma\mathcal{H}\Gamma^{-1} = -\mathcal{H}$, where the chiral operator $\Gamma = \mathbb{I}\otimes\sigma_z$ with $\mathbb{I}$ and σ_z being the $N \times N$ identity and Pauli matrices. This implying that the zero-energy edge state is not affected by such disorder.

In Fig. S8(a), we plot the energy spectra of the disordered Hamiltonian (5) in the main text with $W = 0.5$. It can be seen that zero-energy edge state is insensitive to imperfection in the coupling strengths. In Fig. S8(b), we further calculate the transfer efficiency as a function of the disorder strength. It is found that the transfer efficiency almost remains unchanged for the weak disorder. These results indicate the robustness of the edge-to-edge topological transport. When further increasing the disorder strength, the energy gap gradually decreases [see Fig. S9(a)-(c)], indicating the breakdown of the adiabaticity. As a result, the transfer efficiency decreases rapidly.

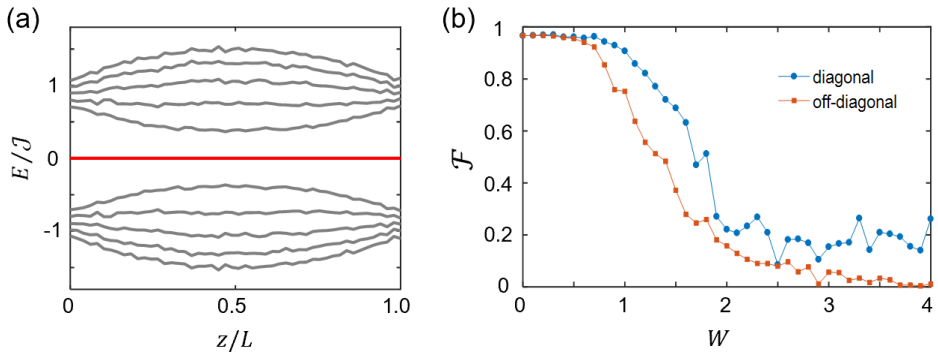

Figure S8. Energy spectra of the exponential modulation of the coupling strengths [Eq. (S14)] with $W = 0.5$ [Hamiltonian (5) in the main text]. (b) The disorder-averaged transport efficiencies $\mathcal{F}$ as functions of W for the off-diagonal and diagonal disorders, when $L = 5$ cm. The site is chosen as 11. (a) and (b) are the disorder-averaged results by choosing 50 samples.

In the presence of the diagonal disorder (on-site energies), the perturbed Hamiltonian (5) of the main text becomes

$$\mathcal{H} = H(z) + \sum_n \mathcal{J}\left(\bar{J}_{1,n}|n,A\rangle\langle n,A| + \bar{J}_{2,n}|n,B\rangle\langle n,B|\right). \quad \text{(S16)}$$

In this case, the perturbed Hamiltonian $\mathcal{H}_d$ does not obey the chiral symmetry and the energy of the edge mode in the gap is modified, as shown in Figs. S9(d)-(f). However, the main influence of this diagonal disorder on the edge-to-edge topological transport is similar to that of the off-diagonal disorder [see Fig. S8(b)]. Especially, for the weak

disorder the transfer efficiency also almost remains unchanged.

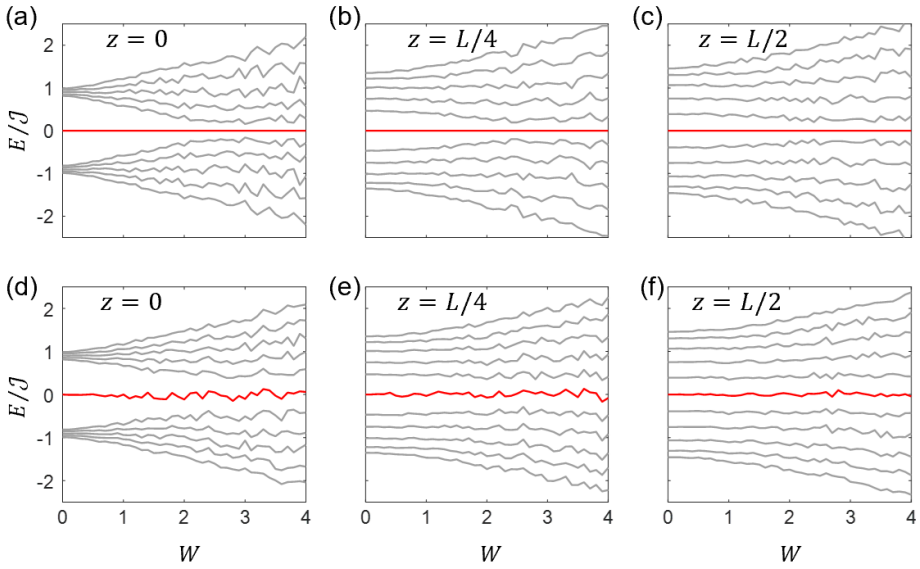

Figure S9. The disorder-averaged energy spectra of exponential modulations as functions of W for the off-diagonal disorders with $z = 0$ (a), $z = L/4$ (b), $z = L/2$ (c). (d-f) The same as (a-c) but for the diagonal disorder. The site is chosen as 11.

SM-VII. Comparison with conventional topological pumping schemes

In this section, we compare the speeds of edge-to-edge transport for three different models, including the Rice-Mele, Aubry-André, and our considered odd-sized SSH models. The Rice-Mele and Aubry-André models are also used to realize adiabatic pumpings.

The Rice-Mele model has the following Hamiltonian [S5]

$$H_{\mathrm{RM}}(z) = \sum_n [J_1(z)|n,A\rangle\langle n,B| + J_2(z)|n+1,A\rangle\langle n,B| + \mathrm{H.c.}] + \sum_n \delta(z)(|n,A\rangle\langle n,A| - |n,B\rangle\langle n,B|), \quad \text{(S17)}$$

which is a modified SSH model with even number of site and staggered potential energies $\pm\delta$. The off-diagonal Aubry-André model has the following Hamiltonian [S6]

$$H_{\mathrm{AA}}(z) = \sum_n \{t[1 + \lambda\cos(2\pi\beta n + \phi(z))]|n+1\rangle\langle n| + \mathrm{H.c.}\}, \quad \text{(S18)}$$

where $\beta = (\sqrt{5}+1)/2$.

Figure S10 shows the energy spectra of the Rice-Mele [Fig. S10(a)], Aubry-André [Fig. S10(b)], and exponential modulated odd-sized SSH [Fig. S10(c)] models. It is found that the edge states are contact with the bulk states for the Rice-Mele and Aubry-André models, while a finite energy gap is always present for our odd-sized SSH model.

In Fig. S11, we further calculate the transport efficiency $\mathcal{F}$ for these three models. It is clear that our scheme possesses higher transport speed.

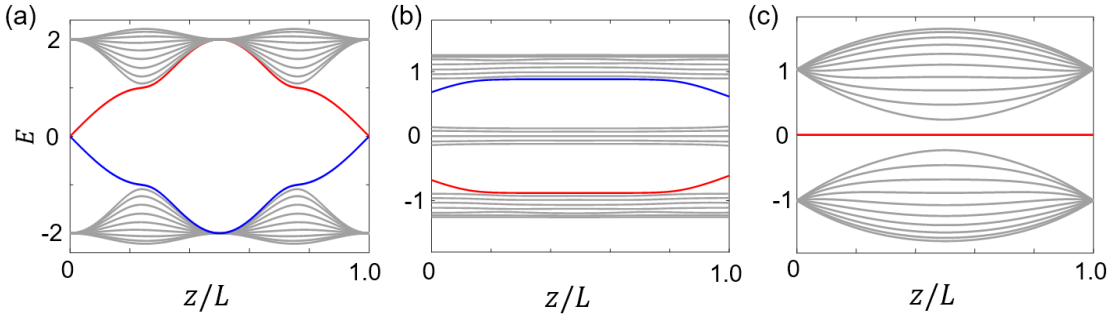

Figure S10. The energy spectra of the Hamiltonian (S17) with $J_1 = 0.5[1 + \cos(2\pi z/L)]$, $J_2 = 0.5[1 - \cos(2\pi z/L)]$ and $\delta = \sin(2\pi z/L)$ (a), the Hamiltonian (S18) with $t = 0.625$, $\lambda = 0.6$ and $\phi(z) = 1.4\pi z/L + 0.35\pi$ (b), and our considered odd-sized SSH lattice (denoted by H_{ODD} for simplicity) with $J_1 = \left(1 - e^{-3z/L}\right)/(1 - e^{-3})$ and $J_2 = \left[1 - e^{-3(L-z)/L}\right]/(1 - e^{-3})$ (c). The sites number is chosen 20 for (a) and 21 for (b) and (c). In all subfigures, the maximum coupling strength is set to 1 and we set it as the energy unit. The red and blue lines denote the edge states.

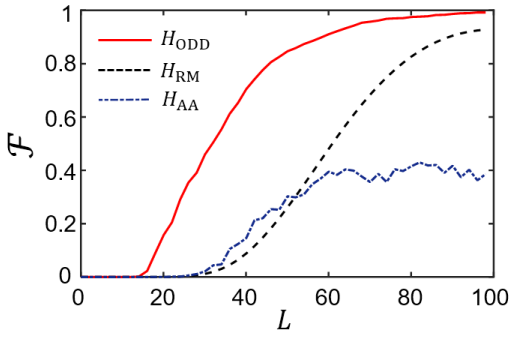

Figure S11. The transport efficiencies $\mathcal{F}$ as functions of L for different pumping schemes. The parameters are the same as those in Fig. S10.

References

[S1] A. Coutant, V. Achilleos, O. Richoux, G. Theocharis, and V. Pagneux, Robustness of topological corner modes against disorder with application to acoustic networks, Phys. Rev. B **102**, 214204 (2020).

[S2] N. E. Palaiodimopoulos, I. Brouzos, F. K. Diakonos, and G. Theocharis, Fast and robust quantum state transfer via a topological chain, Phys. Rev. A **103**, 052409 (2021).

[S3] O. Zilberberg, S. Huang, J. Guglielmon, M. Wang, K. P. Chen, Y. E. Kraus, and M. C. Rechtsman, Photonic topological boundary pumping as a probe of 4D quantum Hall physics, Nature (London) **553**, 59 (2018).

[S4] A. Szameit, F. Dreisow, T. Pertsch, S. Nolte, and A. Tünnermann, Control of directional evanescent coupling in fs laser written waveguides, Opt. Express **15**, 1579 (2007).

[S5] J. K. Asbóth, L. Oroszlány, and A. Pályi, A Short Course on Topological Insulators, Lecture Notes in Physics (Springer, 2016).

[S6] Y. E. Kraus, Y. Lahini, Z. Ringel, M. Verbin, and O. Zilberberg, Topological States and Adiabatic Pumping in Quasicrystals, Phys. Rev. Lett. **109**, 106402 (2012).